

Article

# Glucose-6-Phosphate Dehydrogenase Enhances Antiviral Response through Downregulation of NADPH Sensor HSCARG and Upregulation of NF- $\kappa$ B Signaling

Yi-Hsuan Wu <sup>1,†</sup>, Daniel Tsun-Yee Chiu <sup>1,2,3,†</sup>, Hsin-Ru Lin <sup>4</sup>, Hsiang-Yu Tang <sup>2</sup>, Mei-Ling Cheng <sup>1,2,5</sup> and Hung-Yao Ho <sup>1,2,\*</sup>

Received: 7 October 2015; Accepted: 10 December 2015; Published: 17 December 2015

Academic Editor: Curt Hagedorn

<sup>1</sup> Department of Medical Biotechnology and Laboratory Science, College of Medicine, Chang Gung University, Tao-yuan 333, Taiwan; yihswanwu@mail.cgu.edu.tw (Y.-H.W.); dtychiu@mail.cgu.edu.tw (D.T.-Y.C.); chengm@mail.cgu.edu.tw (M.-L.C.)

<sup>2</sup> Healthy Aging Research Center, Chang Gung University, Tao-yuan 333, Taiwan; tangshyu@gmail.com

<sup>3</sup> Department of Laboratory Medicine, Chang Gung Memorial Hospital, Lin-Kou 333, Taiwan

<sup>4</sup> Molecular Medicine Research Center, Chang Gung University, Tao-yuan 333, Taiwan; rebecca19852006@hotmail.com

<sup>5</sup> Department of Biomedical Sciences, College of Medicine, Chang Gung University, Tao-yuan 333, Taiwan

\* Correspondence: hoh01@mail.cgu.edu.tw; Tel./Fax: +886-3-211-8449

† These authors contributed equally to this work.

**Abstract:** Glucose-6-phosphate dehydrogenase (G6PD)-deficient cells are highly susceptible to viral infection. This study examined the mechanism underlying this phenomenon by measuring the expression of antiviral genes—tumor necrosis factor alpha (*TNF- $\alpha$* ) and GTPase myxovirus resistance 1 (*MX1*)—in *G6PD*-knockdown cells upon human coronavirus 229E (HCoV-229E) and enterovirus 71 (EV71) infection. Molecular analysis revealed that the promoter activities of *TNF- $\alpha$*  and *MX1* were downregulated in *G6PD*-knockdown cells, and that the I $\kappa$ B degradation and DNA binding activity of NF- $\kappa$ B were decreased. The HSCARG protein, a nicotinamide adenine dinucleotide phosphate (NADPH) sensor and negative regulator of NF- $\kappa$ B, was upregulated in *G6PD*-knockdown cells with decreased NADPH/NADP<sup>+</sup> ratio. Treatment of *G6PD*-knockdown cells with siRNA against *HSCARG* enhanced the DNA binding activity of NF- $\kappa$ B and the expression of *TNF- $\alpha$*  and *MX1*, but suppressed the expression of viral genes; however, the overexpression of *HSCARG* inhibited the antiviral response. Exogenous G6PD or IDH1 expression inhibited the expression of *HSCARG*, resulting in increased expression of *TNF- $\alpha$*  and *MX1* and reduced viral gene expression upon virus infection. Our findings suggest that the increased susceptibility of the *G6PD*-knockdown cells to viral infection was due to impaired NF- $\kappa$ B signaling and antiviral response mediated by *HSCARG*.

**Keywords:** G6PD; NADPH; coronavirus; enterovirus; antiviral response; HSCARG

## 1. Introduction

Glucose-6-phosphate dehydrogenase (G6PD) deficiency is the most common enzymopathy in humans, affecting 400 million people worldwide [1]. G6PD plays an essential role in the pentose phosphate shunt for reducing nicotinamide adenine dinucleotide phosphate (NADP<sup>+</sup>) to NADPH. NADPH primarily serves to reduce equivalents for numerous biochemical reactions such as reductive biosynthesis, glutathione reduction, detoxification, and NADPH oxidase-mediated superoxide production. Therefore, G6PD helps to maintain cellular redox homeostasis [2,3], whereas G6PD

deficiency predisposes cells to increased oxidative stress. *G6PD*-knockdown cells exhibit premature senescence, growth retardation, and increased susceptibility to stress-induced apoptosis [4–6]. Clinically, in addition to the classical association with hemolytic anemia [7,8], patients with *G6PD*-deficiency have an increased risk of degenerative diseases [9–12]. *G6PD*-deficient cells are more susceptible to enterovirus, coronavirus, and dengue virus infections [13–15]. These findings suggest that the *G6PD* status, and hence the redox environment, is a risk factor for viral infection. The mechanism underlying the effect of the redox environment on viral replication remains elusive.

Viral replication and spread is inhibited by the antiviral defense mechanisms of the host. The replication and spread normally involves activation of the antiviral innate immune responses and culminates in the production of type I interferons (IFNs) [16] and proinflammatory cytokines such as tumor necrosis factor alpha (TNF- $\alpha$ ) [17,18]. Both IFNs and TNF- $\alpha$  are antiviral cytokines and display strong antiviral activity in host innate immunity [19]. Type I IFNs are the principal antiviral cytokines produced during the innate immune responses to viral infections, and upregulate antiviral proteins [20–22]. More than 300 IFN-stimulated genes (ISGs), which are initiated by type I IFN signaling, have been discovered. Some ISG-encoded proteins, such as GTPase myxovirus resistance 1 (MX1) [23], protein kinase R (PKR) [24], and 2'-5'-oligoadenylate synthetase (OAS) [25], are implicated in the antiviral state. Several ISGs are upregulated by infection with coronavirus or enterovirus [26–28]. TNF- $\alpha$  inhibited viral infections [19], and endogenous TNF- $\alpha$  inhibited the enhanced susceptibility to infectious diseases [29].

Reactive oxygen species (ROS) play crucial roles in many cellular processes including cell proliferation, differentiation, apoptosis, and signal transduction [30–32]. ROS have also been shown to trigger the signaling process of innate immune responses [33,34]. Oxidative stress affects viral replication partly by altering host immunity [35,36]. The inhibitory effect of the *G6PD* status on viral replication is unknown, which can be attributed to the alteration of the host innate immune response from modulating the redox homeostasis of the host cells.

HSCARG, also called NMRAL1, is an NADPH sensor; changes in the NADPH/NADP<sup>+</sup> ratio can induce allosteric change and the subcellular redistribution of HSCARG [37,38]. HSCARG regulates the proteolysis of RelA and the phosphorylation of IKK $\beta$  [39] and plays an essential role in NF- $\kappa$ B signaling [39–41]. Moreover, HSCARG suppresses the TNF- $\alpha$ -stimulated activation of NF- $\kappa$ B [40], suggesting that the NADPH/NADP<sup>+</sup> ratio or the redox status affects the NF- $\kappa$ B-mediated immune response through the modulation of HSCARG. HSCARG can inhibit TRAF3 ubiquitination and negatively regulate the cellular antiviral response [42]. Because of the crucial role of *G6PD* in maintaining cellular NADPH/NADP<sup>+</sup>, examining the relationship among the *G6PD* status, HSCARG, and host innate immune response is worthwhile.

This study addresses how the *G6PD* status affects the innate immune response to viral infection. The expression of viral genes is substantially higher in *G6PD*-knockdown cells infected with human coronavirus strain 229E (HCoV-229E) and EV71 than in infected control cells. The expression of antiviral genes, such as *MX1* and *TNF- $\alpha$* , is upregulated, albeit to lower levels, in *G6PD* deficient cells. HSCARG, whose expression is enhanced in *G6PD*-deficient cells, inhibits I $\kappa$ B degradation and the DNA binding activity of NF- $\kappa$ B. Exogenous *G6PD* or isocitrate dehydrogenase 1 (IDH1), which increases cellular NADPH/NADP<sup>+</sup>, restores NF- $\kappa$ B-mediated antiviral response. These findings demonstrate that *G6PD* activity, and hence NADPH/NADP<sup>+</sup> status, can affect antiviral immunity through the modulation of HSCARG and the NF- $\kappa$ B signaling cascade.

## 2. Materials and Methods

### 2.1. Materials

The following antibodies were used: anti-*G6PD* (Genesis Biotech, Taiwan), anti-His tag, anti-I $\kappa$ B, anti-IDH1, anti- $\beta$ -actin, anti-HSCARG, antihorseradish peroxidase (HRP)-conjugated antimouse IgG, and antirabbit IgG (Santa Cruz Biotechnology, Santa Cruz, CA, USA). TNF- $\alpha$  siRNA, HSCARG siRNA, and nontargeting siRNA were purchased from Dharmacon RNA Technologies (Lafayette, CO, USA).

The ELISA kit for TNF- $\alpha$  was purchased from R & D systems (Minneapolis, MN, USA). BAY 11-7085 and all other chemicals were purchased from Sigma-Aldrich (St. Louis, MO, USA).

## 2.2. Cell Culture

A549 cells (human alveolar epithelial cell carcinoma), MRC-5 cells (human lung fibroblasts), and RD cells (human rhabdomyosarcoma) were purchased from the American Type Culture Collection (ATCC) (Manassas, VA, USA). The cells were cultured in Dulbecco modified Eagle medium supplemented with 10% fetal bovine serum and antibiotics (100 U/mL of penicillin and 100  $\mu$ g/mL of streptomycin) at 37 °C in a humidified 5% CO<sub>2</sub> atmosphere. The cassette for expressing G6PD and scrambled control (Sc) shRNA has been described previously [6]. The cassette was subcloned in pSuperior (Oligoengine, Seattle, WA, USA). The retroviral vectors were packaged into amphotropic virus by using PT67 cells, as previously prescribed [6]. The A549 cells were transduced with the packaged virus and selected for stable transfectants in a medium containing puromycin (2  $\mu$ g/mL).

## 2.3. G6PD Activity

G6PD activity was measured spectrophotometrically at 340 nm according to the reduction of NADP<sup>+</sup> in the presence of glucose-6-phosphate, as previously described [43]. In brief, the cells were collected and resuspended in lysis buffer (50 mM Tris-HCl (pH 7.4), 1% Triton X-100, 0.05% SDS, 150 mM NaCl, 1 mM EGTA, and 1 mM NaF). Cell lysates were centrifuged, and the supernatant was used in the assay. G6PD activity was analyzed by combining the protein and assay buffer (50 mM Tris-HCl (pH 8), 50 mM MgCl<sub>2</sub>, 4 mM NADP<sup>+</sup>, and 4 mM glucose 6-phosphate).

## 2.4. Virus Preparation and Plaque Assay

HCoV-229E was provided by Lai MM (Academia Sinica, Taiwan). The strain was propagated in the MRC-5 cells and purified through centrifugation. The lung carcinoma cell line A549 was used for the plaque assay. The viral titer was calculated according to the plaque formation on the A549 cells, as described previously [14]. Human enterovirus 71 (BrCr strain) was purchased from the ATCC (VR784). The virus was propagated, and plaque formation was assayed on the RD cells. The virus was aliquoted, quick-frozen on dry ice, and stored at –70 °C until used.

## 2.5. Quantitative-PCR

Total RNA was isolated using Trizol reagent. cDNA was performed using the SuperScript III system (Invitrogen, Carlsbad, CA, USA). Primers were designed according to the sequences of human antiviral gene cDNAs and those of viral genes. The sequences of the primers used in RT-PCR are listed in Table S1. Quantitative-PCR was performed using the IQ<sup>TM</sup> SyBr Green Supermix kit on an IQ5 Real Time Thermal Cycler (Bio-Rad, Hercules, CA, USA). Relative fold expression values were determined using the  $\Delta\Delta$ Ct method.

## 2.6. Preparation of Cell Extracts and Western Blot Analysis

The cells were washed with ice-cold phosphate-buffered saline (PBS), scraped in lysis buffer (20 mM Tris-HCl (pH 7.5), 150 mM NaCl, 1% Nonidet P-40, 1 mM EDTA, 10  $\mu$ g/mL aprotinin, 10  $\mu$ g/mL leupeptin, 1 mM phenylmethylsulfonyl fluoride), and centrifuged at 40,000 $\times$  g for 30 min at 4 °C to yield the whole-cell extract. Samples were denatured, electrophoresed on 10% SDS-polyacrylamide gel, and transferred to polyvinylidene difluoride (PVDF) membranes. The membranes were incubated overnight at 4 °C with an appropriate dilution of a primary antibody (1:1000) in Tris-buffered saline (TBS) (50 mM Tris-HCl, 150 mM NaCl, 0.05% (w/v) Tween-20 (pH 7.4)) containing 5% (w/v) bovine serum albumin (BSA). Membranes were incubated with a 1:4000 dilution of antirabbit or antimouse-HRP antibody for 1.5 h. The immunoreactive bands were visualized by ECL reagents (GE Healthcare, Little Chalfont, Buckinghamshire, UK), with the signals captured by exposure to X-ray film.

### 2.7. Plasmid Construction

The cDNA encoding His-tagged G6PD (Accession No. NM\_000402), IDH1 (Accession No. NM\_005896), and HSCARG (Accession No. NM\_001305141.1) were cloned in pCI-neo plasmid (Invitrogen). The promoter region of the *TNF- $\alpha$*  and *MX1* gene was cloned from human genomic DNA, and subcloned in a pGL3-basic vector (Promega, Mannheim, Germany). A *MX1* promoter region devoid of NF- $\kappa$ B binding site (–244 to –235) was engineered. Mutant (–242 to –239; MX1P-mut; MX1M) and deletion (–244 to –235; MX1P-del; MX1D) forms of *MX1* promoter were established by site-directed mutagenesis (Stratagene, Amsterdam, Netherlands).

### 2.8. Transfection of Plasmids or siRNAs

The A549 cells ( $5 \times 10^5$ ) were seeded on six-well plates and transfected 24 h later with plasmids using Lipofectamine 2000 (Invitrogen). During transient transfection with siRNA, the cells were transfected with 10 nM TNF- $\alpha$  or HSCARG siRNA. The nontargeting siRNA was used as a control for nonspecific effects of transfected siRNA. During transient transfection with plasmid, the cells were transfected according to the standard protocol (Invitrogen, CA, USA). The cells were harvested for analysis, or infected with HCoV-229E, 24 h after transfection.

### 2.9. Electrophoretic Mobility Shift Assay

G6PD-knockdown (Gi) and Sc A549 cells were infected with HCoV-229E for the indicated periods. Nuclear proteins were extracted using the Nuclear Extract kit (Active Motif, Carlsbad, CA, USA). Electrophoretic mobility shift assays (EMSAs) were carried out using the LightShift Chemiluminescent EMSA kit according to manufacturer protocol (Thermo Scientific, Rockford, IL, USA). In brief, the extract (10  $\mu$ g) was incubated for 1 h at 4 °C with biotin end-labeled probe (Thermo Scientific, Rockford, IL, USA) containing NF- $\kappa$ B DNA-binding sites (5'-AGTTGAGGGGACTTTCCAGGC-3'); the extract was resolved by nondenaturing PAGE on 4% polyacrylamide gel, transferred to nylon plus membrane, and determined by chemiluminescence according to manufacturer instructions.

### 2.10. Luciferase Assay

The A549 cells were transfected with 100 ng of reporter plasmid together with 400 ng of a pRL-null Renilla luciferase-encoding vector by using LF2000 (Invitrogen, Carlsbad, CA, USA). Twenty-four hours later, the A549 cells were infected with HCoV-229E at a multiplicity of infection (MOI) of 0.1. The cellular extract was assayed for luciferase activity using a dual luciferase assay and GLOMAX luminometer (Promega, Madison, WI, USA). Firefly luciferase activity was normalized to Renilla luciferase levels, and is expressed relative to pGL3-basic levels (RLU).

### 2.11. Determination of the NADPH/NADP<sup>+</sup> Ratio

Determination of NADPH and NADP<sup>+</sup> was performed as previously described [44]. In brief, the cells were washed twice with PBS and extracted in 80% methanol/10 mM KOH solution. After centrifugation at 14,000 $\times$  g for 5 min, the supernatant was retained and completely dried under nitrogen gas. The sample was analyzed using ultra performance liquid chromatography (UPLC) equipped with a photodiode array detector. The sample was chromatographed on an Acquity HSST3 reversed-phase C18 column (2.1 mm  $\times$  150 mm, particle size of 1.8 mm; Waters Corp., Milford, MA, USA). The mobile phase was composed of 25 mM potassium monobasic phosphate buffer, pH 6 (solvent A), and 100% methanol (solvent B). The mobile phase conditions were as follows: solvent A, 2 min, gradient from 0 to 3%; solvent B, 0.5 min, gradient from 3% to 4%; solvent B, 2.5 min, gradient from 4% to 15%; solvent B, 2 min, gradient 15%; and solvent B, 1 min. The column temperature was maintained at 37 °C. The flow rate was set at 0.38 mL/min. Absorbance spectra were acquired over the wavelength range from 260 to 340 nm.

## 2.12. Statistical Analysis

Statistical analyses were carried out using a two-tailed Student's *t* test. A *p* value of  $\leq 0.05$  was considered statistically significant. The data were representative of at least three independent experiments, and the values were given as the mean of replicate experiments  $\pm$  standard deviation (SD).

## 3. Results

### 3.1. G6PD Deficiency Impairs the Expression of the Antiviral Genes, *TNF- $\alpha$* and *MX1*, upon HCoV-229E or EV71 Infection

The A549 cells were infected with a retroviral vector expressing G6PD-specific (Gi) and Sc shRNA. The generated A549-Gi and A549-Sc were used to delineate the mechanism underlying the increased susceptibility of G6PD-deficient cells to viral infection. The expression of G6PD was significantly reduced in A549-Gi cells compared with the A549-Sc cells (Figure 1A, top panel). The A549-Gi cells were infected with the HCoV-229E virus at a MOI of 0.1. The titer of progeny virus derived from the infected A549-Gi cells was significantly higher compared with the infected A549-Sc cells (Figure 1A, bottom panel). These findings are consistent with the temporal change in the expression of the viral *N* gene. The expression of the *N* gene increased with the time of infection (Figure 1B), and was higher in the A549-Gi cells than in the A549-Sc cells. The *N* gene level increased 304-fold in the A549-Gi cells versus an increase of 106-fold in the A549-Sc cells at 8 h postinfection (p.i.). At 24 h p.i., there was an over 17,000-fold increase in the *N* gene level in the A549-Gi cells and 5,000-fold increase in the A549-Sc cells. These findings are consistent with our previous findings [14].

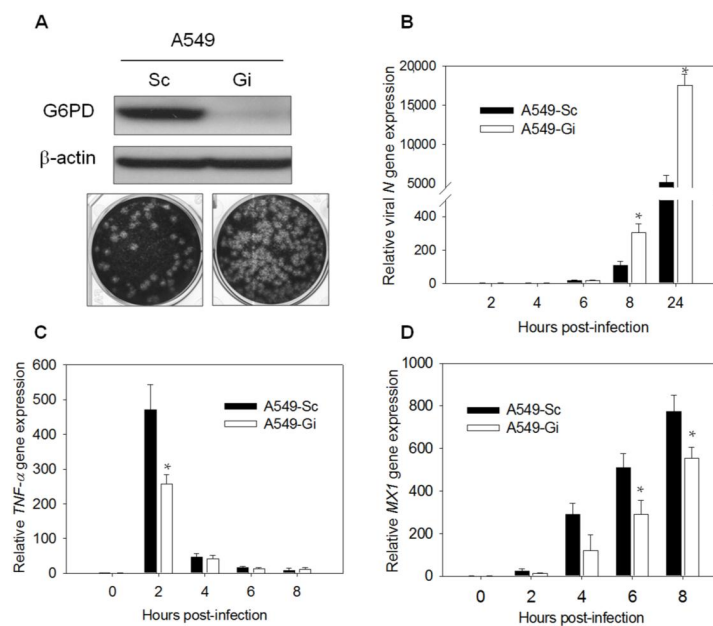


**Figure 1.** Expressions of antiviral gene *MX1* and *TNF- $\alpha$*  decrease upon HCoV 229E infection in A549-Gi cells. (A) A549-Sc and -Gi cells were harvested for determination of G6PD expression by western blotting.  $\beta$ -Actin was used as internal control. A549-Sc and -Gi cells were infected with HCoV-229E (0.1 MOI) for 24 h then viral particle was harvested and production was determined using plaque assay; (B) A549-Sc and -Gi cells were infected with HCoV-229E (0.1 MOI) for indicated time points. Viral *N* gene expression was determined by quantitative-PCR. Data were normalized to the value of infected A549-Sc cells at 2 h p.i.; (C) RNA was harvested from HCoV-229E-infected cells at indicated time p.i.. *TNF- $\alpha$*  gene expression was determined by quantitative-PCR. Data were normalized to the value of uninfected A549-Sc cells; (D) RNA was harvested from HCoV 229E-infected cells at indicated time points p.i.. *MX1* gene expression was determined by quantitative-PCR. Data were normalized to the value of uninfected A549-Sc cells. Values represent average  $\pm$  SD of three experiments. \* *p* < 0.05 as compared to A549-Sc cells.

The discrepancy between the viral replication in normal cells and G6PD-deficient cells correlates with their antiviral gene expression. Numerous antiviral genes were found to be upregulated in the A549 and MRC-5 cells after infection with HCoV-229E (Table 1). The expression of the antiviral genes *TNF- $\alpha$*  and *MX1* was studied in the infected A549-Gi and A549-Sc cells. *TNF- $\alpha$*  mRNA levels increased more than 400-fold in the A549-Sc cells at 2 h p.i., and returned to the original levels at 8 h p.i. (Figure 1C). The induction level was considerably lower in the A549-Gi cells, with the mRNA levels showing only a 250-fold increase at 2 h p.i. (Figure 1C, white bars). Likewise, the expression of the *MX1* gene increased during the infection course of HCoV-229E, and was significantly higher in the A549-Sc cells than in the A549-Gi cells (Figure 1D). The level of *MX1* mRNA increased over 22.8-fold at 2 h p.i. and 774.2-fold at 8 h p.i in the A549-Sc cells (Figure 1D). However, the level of induction was also reduced by 40% at 2 h p.i. and by 28% at 8 h p.i in the A549-Gi cells. The difference in inducibility of antiviral genes in control versus G6PD-deficient cells was observed in the case of EV71 infection, which increased *TNF- $\alpha$*  and *MX1* expression in RD cells (Table S2 and Figure S1). The expression of *TNF- $\alpha$*  (Figure S1B) and *MX1* (Figure S1C) genes in *G6PD*-knockdown RD-Gi cells was significantly lower than in RD-Sc cells. Furthermore, *G6PD*-knockdown increased the susceptibility to EV71 infection (Figure S1A, right panel; *G6PD* protein expression was shown in the left panel). These findings suggest that the expression of *TNF- $\alpha$*  and *MX1* is suppressed in G6PD-deficient cells.

### 3.2. *TNF- $\alpha$* Knockdown Enhances Viral Replication in A549 Cells

*TNF- $\alpha$*  is implicated in the modulation of the viral life cycle and the regulation of antiviral gene expression [17]. To test whether *TNF- $\alpha$*  expression limits virus replication, we knocked down *TNF- $\alpha$*  expression in A549 cells and examined their viral susceptibility. Pretreatment of the A549 cells with siRNA against *TNF- $\alpha$*  significantly reduced HCoV-229E-induced *TNF- $\alpha$*  expression throughout the course of infection (Figure 2A). Moreover, there was an increase in viral gene expression (Figure 2B). Conversely, *TNF- $\alpha$*  pretreatment significantly inhibited viral replication in a dose dependent manner (Figure 2C). These findings suggest that *TNF- $\alpha$*  plays a determinant role in the antiviral response. The reduced inducibility in G6PD-deficient cells may account for the increase in the viral replication of these cells.

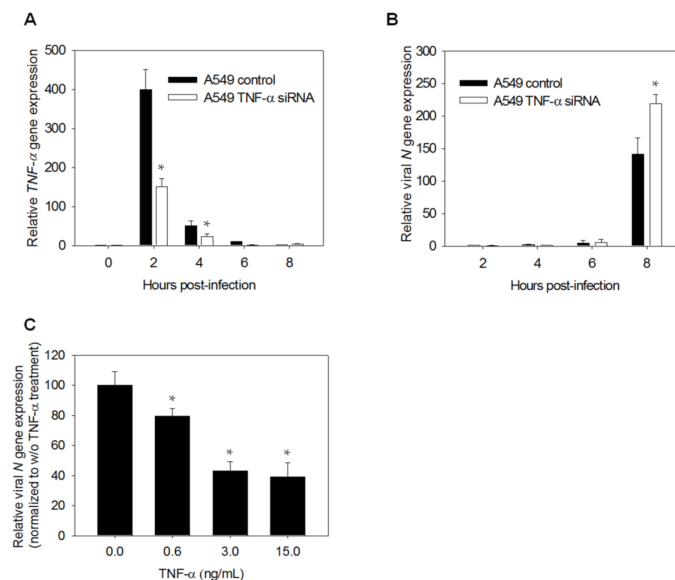


**Figure 2.** *TNF- $\alpha$*  inhibits viral replication in A549 cells. (A,B) The A549 cells were treated with control or *TNF- $\alpha$*  siRNA for 24 h and challenged with HCoV 229E of 0.1 MOI. Total RNA was harvested at indicated time and analyzed for *TNF- $\alpha$*  mRNA and viral *N* gene expression; (C) The A549 cells were challenged with different concentration of *TNF- $\alpha$*  for 24 h then infected with HCoV 229E of 0.1 MOI for 8 h. Total RNA was harvested for analyzing viral *N* gene expression by quantitative-PCR. Values represent average  $\pm$  SD of three measurements. \*  $p < 0.05$ , as compared to control siRNA-treated cells.

**Table 1.** Time course pattern of antiviral gene expression in the A549 and MRC-5 cells upon HCoV 229E infection.

Cell Type	Gene	Fold Increase						
		0 h	2 h	4 h	6 h	8 h	10 h	24 h
A549	HCoV 229E N gene	N.D.	1	5.08 ± 1.30	20.92 ± 6.45	102.73 ± 15.24	946.55 ± 83.16	5566.24 ± 312.68
	<i>TNF-α</i>	1	432.58 ± 23.35	71.32 ± 0.41	27.05 ± 0.89	8.39 ± 1.29	7.71 ± 0.75	236.52 ± 33.27
	<i>IFN-α</i>	1	0.89 ± 0.11	1.76 ± 0.83	1.29 ± 0.43	2.30 ± 1.14	1.90 ± 0.87	5.27 ± 1.73
	<i>IFN-β</i>	1	1.31 ± 0.09	1.17 ± 0.15	1.43 ± 0.27	0.86 ± 0.29	1.81 ± 0.35	504.07 ± 42.68
	<i>OAS</i>	1	1.77 ± 0.32	5.49 ± 0.22	9.73 ± 0.42	11.64 ± 2.53	15.16 ± 2.15	27.1 ± 1.25
	<i>PKR</i>	1	8.99 ± 2.94	7.45 ± 1.48	7.96 ± 1.51	8.08 ± 1.46	7.47 ± 1.54	8.72 ± 1.97
	<i>MX1</i>	1	123.69 ± 1.09	522.69 ± 50.95	736.82 ± 194.12	1390.95 ± 65.63	2381.91 ± 205.05	3709.11 ± 172.71
MRC-5	HCoV 229E N gene	N.D.	1	1.90 ± 0.12	6.96 ± 1.41	77.96 ± 14.32	311.13 ± 30.21	1145.40 ± 104.50
	<i>TNF-α</i>	1	1441.36 ± 343.85	975.38 ± 63.78	303.71 ± 60.77	137.94 ± 24.09	35.49 ± 2.29	7955.68 ± 664.50
	<i>IFN-α</i>	1	0.78 ± 0.20	0.93 ± 0.32	1.39 ± 0.54	0.79 ± 0.52	1.63 ± 0.24	0.88 ± 0.43
	<i>IFN-β</i>	1	0.92 ± 0.02	0.89 ± 0.12	0.98 ± 0.29	0.84 ± 0.05	1.23 ± 0.92	1194.91 ± 36.47
	<i>OAS</i>	1	11.27 ± 1.33	93.33 ± 0.41	289.97 ± 27.38	521.57 ± 170.79	997.31 ± 182.12	4775.85 ± 620.45
	<i>PKR</i>	1	4.10 ± 1.84	4.18 ± 1.69	5.16 ± 2.13	4.33 ± 0.24	5.00 ± 1.45	5.07 ± 0.51
	<i>MX1</i>	1	121.73 ± 44.20	512.70 ± 4.42	1345.64 ± 105.59	1774.51 ± 185.55	1966.26 ± 333.56	6117.88 ± 674.95

N. D.: Not Detected.

### 3.3. Transcription of the *TNF- $\alpha$* and *MX1* Genes Is Reduced in G6PD-Knockdown Cells Upon Virus Infection

The effect of the G6PD status on the expression of the *TNF- $\alpha$*  and *MX1* genes may be due to differences between the transcriptional levels of G6PD-knockdown and control cells. To test this hypothesis, A549-Sc and A549-Gi cells were transfected with reporter constructs, which have promoters of the *TNF- $\alpha$*  and *MX1* genes (Figure 3A). The transfected cells were assayed for luciferase activity after infection with HCoV-229E. The *TNF- $\alpha$*  and *MX1* promoter activity in the A549-Sc cells increased significantly at 24 h p.i. compared with that of the mock-infected control (Figure 3B). The promoter activities of the *TNF- $\alpha$*  and *MX1* genes were reduced in the A549-Gi cells. Moreover, lower promoter activities, especially those of the *TNF- $\alpha$*  gene, were observed in the A549-Gi cells compared with the A549-Sc cells under basal conditions. These findings suggest that the transcriptional activities of antiviral genes are affected by the G6PD status.

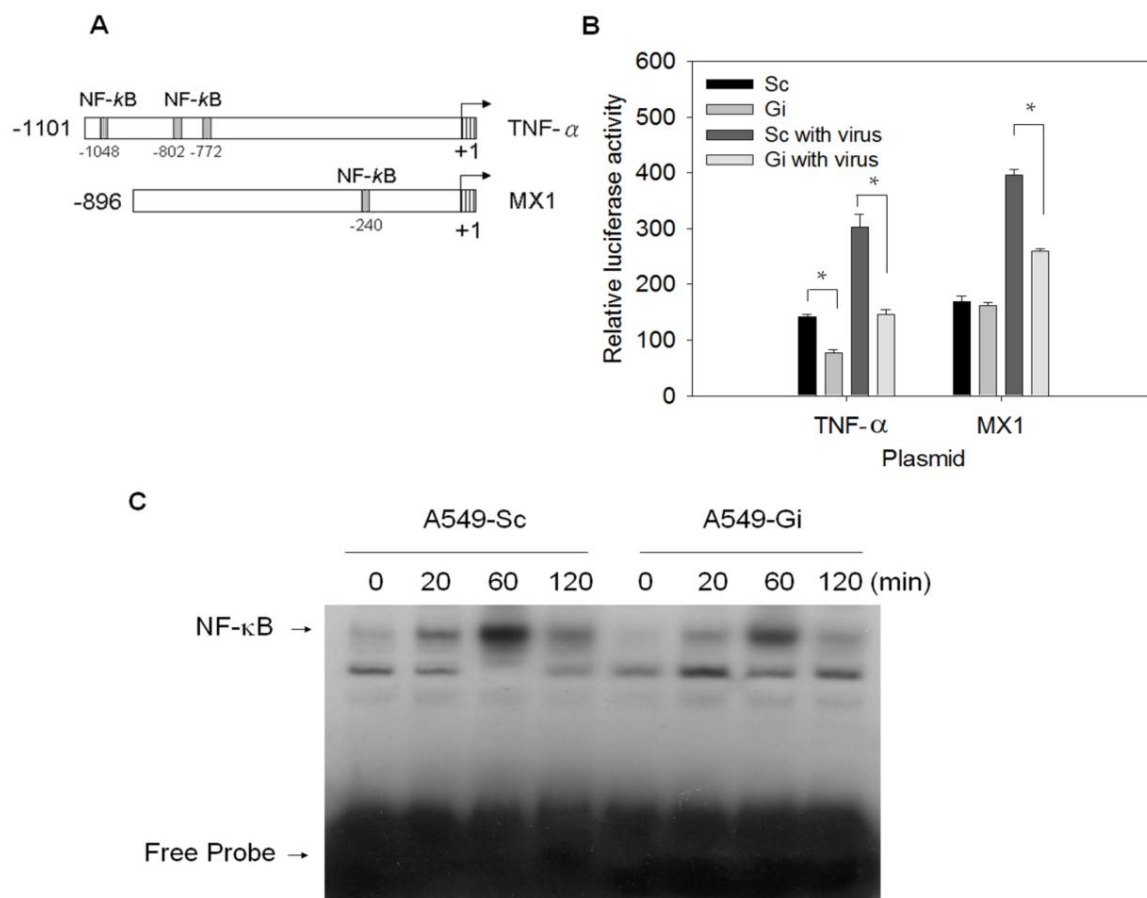


**Figure 3.** Promoter activities of antiviral genes, *TNF- $\alpha$*  and *MX1*, and NF- $\kappa$ B binding activity is highly correlated with G6PD status upon HCoV 229E infection. (A) Schematic presentation of the *TNF- $\alpha$*  (–1 to –1101) and *MX1* (–1 to –896) promoter region are shown. The transcriptional start site is marked with an arrow (+1). NF- $\kappa$ B binding sites are indicated with labeled boxes; (B) A549-Sc and -Gi cells were transfected with control, *TNF- $\alpha$*  and *MX1* reporter plasmid for 24 h, and were untreated or infected with HCoV-229E at MOI of 0.1. Luciferase activity was analyzed at 24 h p. i., and expressed as mean  $\pm$  SD ( $n = 3$ ) of fold change relative to vector control. \*  $p < 0.05$  as A549-Gi cells compared to A549-Sc cells alone or infected with virus, respectively; (C) A549-Sc and -Gi cells were infected with HCoV-229E at MOI of 0.1 for indicated periods. Nuclear extracts were prepared, and DNA binding activity was assayed by EMSA. DNA-protein complexes were resolved by electrophoresis and detected by chemiluminescence.



### 3.4. Binding Activity of NF- $\kappa$ B Is Diminished in Virus-Infected G6PD-Knockdown Cells

Because the NF- $\kappa$ B binding sites were found in *TNF- $\alpha$*  [45] and *MX1* [46] promoter sequences (Figure 3A), G6PD deficiency probably inhibited the expression of these genes by altering the NF- $\kappa$ B signaling. The binding activity of NF- $\kappa$ B increased in the A549-Sc cells upon HCoV-229E infection, reaching the maximal level at 60 min p.i. and decreasing afterwards. The binding activity of NF- $\kappa$ B was higher in the A549-Sc cells than in the A549-Gi cells (Figure 3C). These findings suggest that G6PD deficiency leads to decreased NF- $\kappa$ B activation in virus-infected host cells.

To further confirm the role of NF- $\kappa$ B in the virus-induced upregulation of the *TNF- $\alpha$*  and *MX1* genes, we treated A549 cells with BAY 11-7085, a specific NF- $\kappa$ B inhibitor, and examined the temporal change in the expression of antiviral genes after infection. BAY 11-7085 significantly reduced the induction of the *TNF- $\alpha$*  and *MX1* genes (Figure S2). These data suggest that NF- $\kappa$ B activation is essential to virus-induced antiviral gene expression.

In contrast to the *TNF- $\alpha$*  gene that has the promoter endowed with NF- $\kappa$ B binding sites [45], little is known about the role of NF- $\kappa$ B in *MX1* promoter regulation. The modest increase in the promoter activity of the *MX1* gene raises doubt concerning the involvement of NF- $\kappa$ B in *MX1* promoter regulation. Various reporter vectors containing a luciferase gene linked to various forms of *MX1* gene promoter were constructed, and their activities were examined in the infected cells. The construct MX1P had the wild-type *MX1* gene promoter, while the constructs MX1D and MX1M had no binding sites or had mutant NF- $\kappa$ B binding sites (Figure 4A). HCoV-229E induced significant induction of the MX1P luciferase construct (Figure 4B). By contrast, the luciferase activity of MX1D and MX1M upon HCoV-229E infection was not significantly different from the uninfected control. These findings suggest that NF- $\kappa$ B plays a crucial role in the transcriptional regulation of the *MX1* gene.

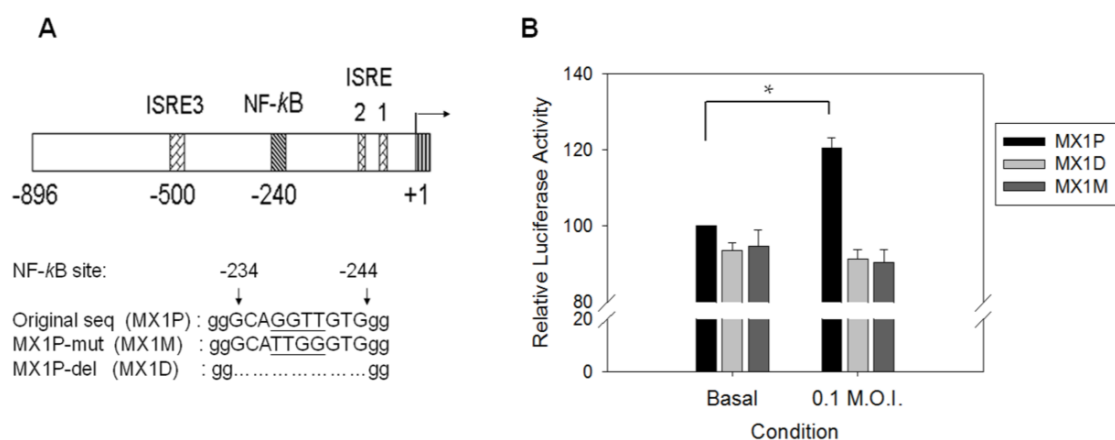


**Figure 4.** The promoter activity of *MX1* gene can be modulated by NF- $\kappa$ B in HCoV 229E-infected cells. (A) Schematic presentation of the *MX1* promoter region (–1 to –896). The transcriptional start site is marked with an arrow (+1). Three ISREs and one NF- $\kappa$ B (–234 to –244) binding site are indicated with labeled boxes. A *MX1* promoter region devoid of NF- $\kappa$ B binding site (–244 to –235) was engineered as described in Materials and Methods. The underlined letters indicates the nucleotides to be changed in MX1M-mut, and the dotted line indicates the nucleotides deleted in MX1P-del; (B) A549 cells were transfected with firefly and Renilla luciferase reporter plasmids containing MX1P, MX1D, or MX1M sequence. Twenty-four hours after transfection, cells were infected with HCoV 229E of 0.1 MOI. Luciferase activities was assayed at 48 h after transfection, and firefly luciferase activity was standardized by Renilla luciferase activity. The values are expressed relative to MX1P under basal condition. \*  $p < 0.05$  as compared to basal condition ones.

### 3.5. HSCARG Expression Is Enhanced in G6PD-Knockdown Cells

HSCARG was proposed as a cellular redox sensor of the NADPH/NADP<sup>+</sup> ratio, and a regulator of NF-κB signaling. HSCARG blocks IκB degradation and inhibits NF-κB activation [39]. The finding revealed a significantly lower NADPH/NADP<sup>+</sup> ratio in A549-Gi cells compared with A549-Sc cells; this increases the possibility that HSCARG is involved in the regulation of NF-κB signaling (Figure 5A). The level of HSCARG transcript was elevated in the A549-Gi cells compared with that of the A549-Sc cells (Figure 5B). In addition, the level of HSCARG protein was higher in the A549-Gi cells than in the A549-Sc cells (Figure 5C). These results suggest that the G6PD status is involved in the regulation of HSCARG expression, thereby affecting NF-κB signaling and antiviral response.

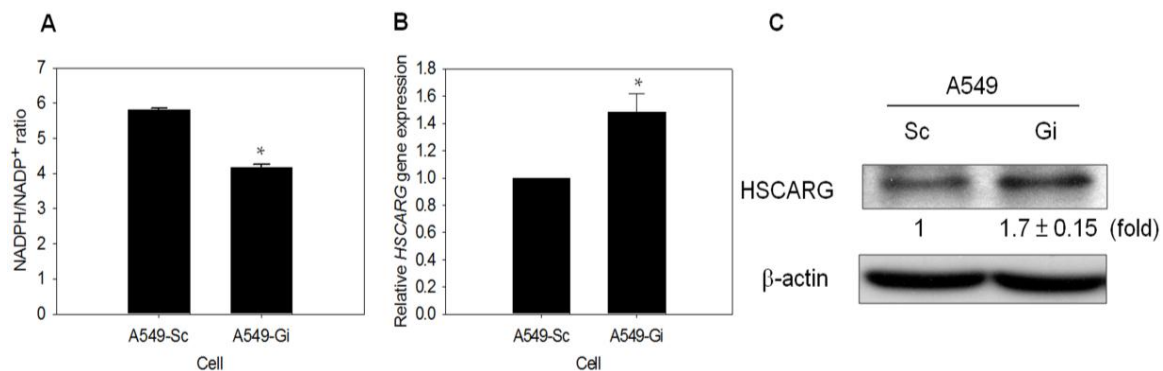


**Figure 5.** Expression of HSCARG increases in G6PD-knockdown A549 cells. (A) NADPH and NADP<sup>+</sup> content were determined by UPLC, and NADPH/NADP<sup>+</sup> ratio was calculated. \*  $p < 0.05$  as compared to A549-Sc cells; (B) The level of HSCARG mRNA was determined in A549-Sc and A549-Gi cells by quantitative-PCR. The level of HSCARG gene expression was normalized to that of A549-Sc cells. \*  $p < 0.05$ , as compared to A549-Sc cells; (C) HSCARG protein in A549-Sc and A549-Gi cells was quantified by western blotting, and β-actin serves as internal control. The relative change in HSCARG protein level is shown as compared to A549-Sc cells. Numbers shown below the upper panel indicate the fold change in HSCARG expression relative to that of Sc cells.

### 3.6. Enhancement of the Antiviral Response and Inhibition of Viral Gene Expression Are Observed in HSCARG-Knockdown Cells

To investigate the role of HSCARG in the antiviral response, A549-Gi cells were transfected with HSCARG-specific siRNA and the nontargeting siRNA control. Treatment of the A549-Gi cells with HSCARG-specific siRNA caused a significant reduction in the level of HSCARG mRNA (Figure 6A). The HSCARG-specific and nontargeting-siRNA-treated cells were infected with HCoV-229E (at a MOI of 0.1), and assayed for NF-κB binding activity. The NF-κB binding activity was enhanced in the HSCARG-specific, siRNA-treated cells. The NF-κB binding activity in these cells was compared with that of the nontargeting siRNA-treated cells (Figure 6B). The effect of the siRNA treatment on the temporal change of the expression of the *TNF-α* and *MX1* genes were studied in the infected cells. The levels of the transcripts of these genes were elevated in the HSCARG-specific, siRNA-treated cells compared with the nontargeting siRNA-treated cells during the course of HCoV-229E infection (Figure 6C,D). The elevation in the expression of the antiviral genes was accompanied by a converse reduction in the expression of the viral *N* gene (Figure 6E). The overexpression of HSCARG in the A549 cells decreased NF-κB binding activity. Therefore, antiviral gene expression increased coronaviral replication (Figure S3). These findings suggest that HSCARG acts diminish NF-κB activation, and suppresses antiviral gene expression in G6PD-knockdown cells.

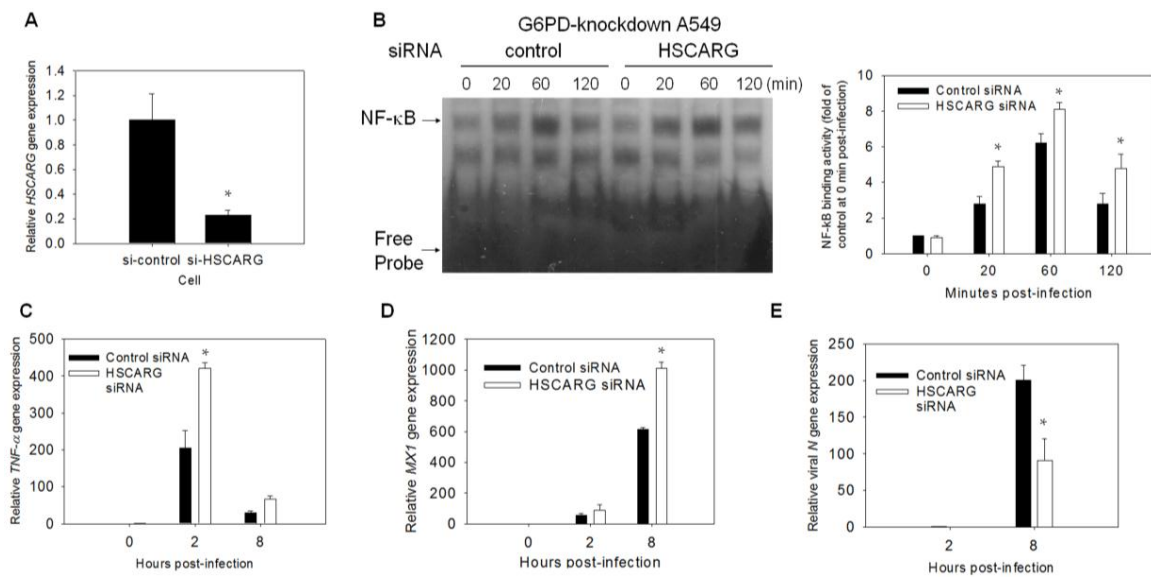


**Figure 6.** *HSCARG*-knockdown increases antiviral response and decreases viral replication. (A,B) A549-Gi cells were transfected with *HSCARG* siRNA. Total RNA was collected at 48 h after transfection, and *HSCARG* gene expression was determined by quantitative-PCR. Level of *HSCARG* was expressed relative to that of A549-Gi cells transfected with control-siRNA. For assay of NF- $\kappa$ B binding activity, A549-Gi cells were transfected with control or *HSCARG* siRNA for 48 h, and subsequently infected with HCoV 229E at MOI of 0.1. At indicated time points p.i., NF- $\kappa$ B binding activity was analyzed by EMSA. The temporal change in NF- $\kappa$ B binding activity is shown and quantified by densitometric scanning. The values represent average  $\pm$  SD of five independent experiments; (C–E) A549-Gi cells were transfected with control or *HSCARG* siRNA for 48 h, and subsequently infected with HCoV 229E at an MOI of 0.1. Total RNA was harvested at indicated time points p.i., and analyzed for expression level of *TNF- $\alpha$*  (C), *MX1* (D), and viral *N* genes (E) by quantitative-PCR. Values represent average  $\pm$  SD of three experiments. \*  $p < 0.05$  as compared to control siRNA treated cells.

### 3.7. Exogenous G6PD or IDH1 Expression Restores Antiviral Gene Expression and Inhibits Viral Replication

As G6PD is indispensable in the maintenance of the redox status [47], it is possible that the alteration of cellular redox status changes *HSCARG* expression. To test this possibility, A549-Gi cells were transfected with constructs encoding His-tagged G6PD and IDH1. The expression of G6PD or IDH1 in the A549-Gi cells led to the diminished expression of the *HSCARG* transcript (Figure 7A,B), and significantly increased NADPH/NADP<sup>+</sup> ratio compared with vector-transfected control cells (Figure 7C). Because knockdown of G6PD expression could suppress antiviral gene expression and enhance *N* gene expression, it would be worthwhile to investigate how exogenous G6PD or IDH1 expression could reverse such changes. Exogenous G6PD or IDH1 expression led to an increase in *TNF- $\alpha$*  and *MX1* gene expression upon HCoV-229E infection (Figure 7D,E). This was accompanied by decreased viral *N* gene expression (Figure 7F). These findings strongly support the notion that cellular G6PD activity and the NADPH/NADP<sup>+</sup> status affect NF- $\kappa$ B signaling by modulating *HSCARG* expression.

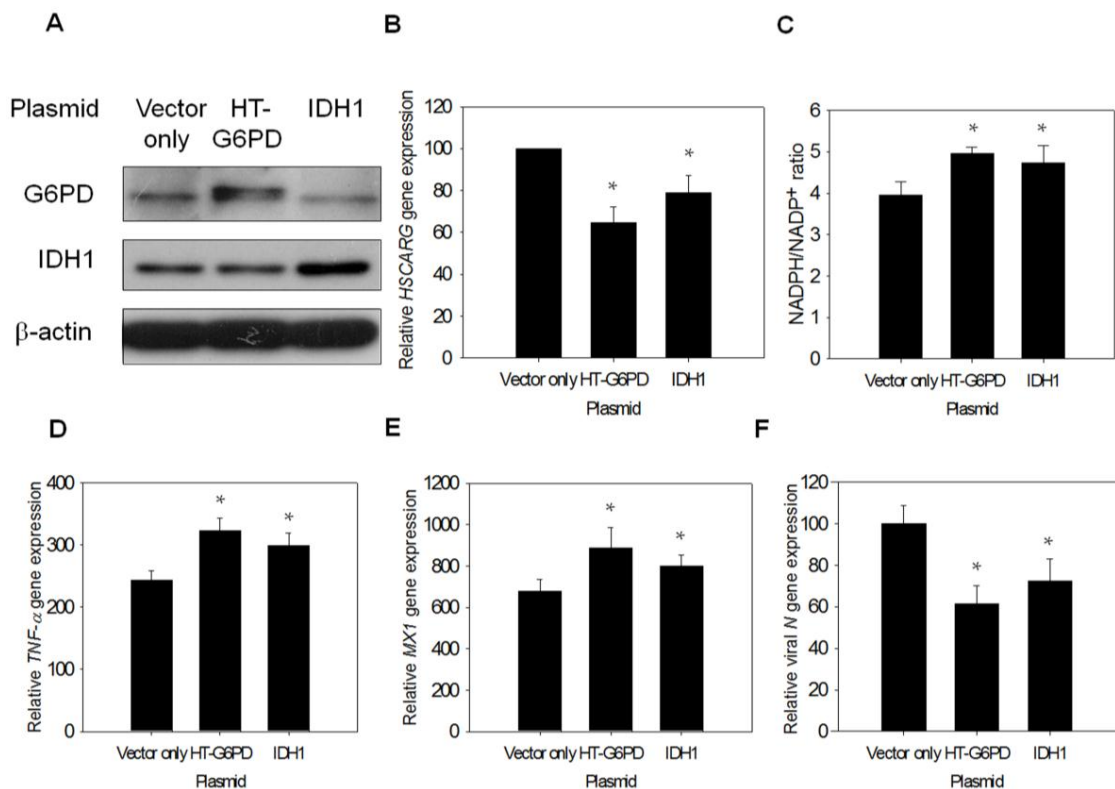


**Figure 7.** Expression of *G6PD* or *IDH1* gene augments antiviral gene expression in HCoV-229E-infected A549-Gi cells. (A,B) A549-Gi cells were transfected with expression construct encoding His-tagged *G6PD* or *IDH1*. Forty-eight hours later, RNA and cell lysate were harvested for analysis. Ectopic protein expression of HT-*G6PD* or *IDH1* was measured by western blot. The level of *HSCARG* gene expression was determined by quantitative-PCR. The level of *HSCARG* gene expression was normalized to that of vector only-transfected cells; (C) NADPH and NADP<sup>+</sup> content were determined by UPLC, and NADPH/NADP<sup>+</sup> ratio was calculated. \*  $p < 0.05$  as compared to vector only control; (D–F) The A549 cells were transfected with expression construct encoding His-tagged *G6PD* or *IDH1*, and cells were infected with HCoV-229E at 0.1 MOI 48 h later; Total RNA was harvested for determination of expression level of *TNF- $\alpha$*  (at 2 h post-infection) (D); *MX1* (at 8 h post-infection) (E) and viral gene (at 8 h post-infection) (F) by quantitative-PCR. Data are expressed relative to that of cells transfected with control vector. Values present the average  $\pm$  SD of three experiments. \*  $p < 0.05$  as compared to vector only-transfected cells.

#### 4. Discussion

This study demonstrates that cellular redox affects viral replication, at least partly, via regulation of the antiviral immune response. The *G6PD* status, a determinant of the NADPH/NADP<sup>+</sup> ratio, affects cellular *HSCARG* expression, and modulates the level of NF- $\kappa$ B activation and the expression of antiviral genes in response to viral infection. Our findings support the notion that a change in the redox status can affect antiviral signaling (Figure 8).

Viruses, such as the influenza virus and the coronavirus, elicit cellular innate immunity [48–52]. We have previously shown that *G6PD*-knockdown cells are more susceptible to viral infection [13,14]. It is probable that the increased susceptibility to viral infections may be partly due to the impaired immune response of *G6PD*-knockdown cells. The expression of cytokine genes (such as *IFN- $\alpha/\beta$*  and *TNF- $\alpha$* ) and antiviral genes (such as *IFN*-stimulated genes (ISGs)) increases in A549 and MRC-5 cells upon HCoV-229E infection, and increases in RD cells upon EV71 infection. The expression of the *TNF- $\alpha$*  and *MX1* genes are differentially regulated in both the normal and *G6PD*-deficient cells, revealing the modulatory effect of cellular redox status on the innate immune system. Consistent with previous

studies reporting that  $TNF-\alpha$  exerts an antiviral effect [17,19,53], the present study demonstrates that  $TNF-\alpha$  protects epithelial cells from HCoV-229E infection. Knockdown of  $TNF-\alpha$  expression can enhance HCoV-229E replication, whereas  $TNF-\alpha$  pretreatment can decrease the susceptibility of infection in *G6PD*-knockdown A549 cells. Moreover, the kinetics of *MX1* gene induction is of particular interest. The *MX1* gene is induced in cells upon infection with HCoV-229E or EV71 at a time point when the type I IFN level is low. These findings suggest that the induction of the *MX1* gene may occur via a type I IFN-independent pathway.

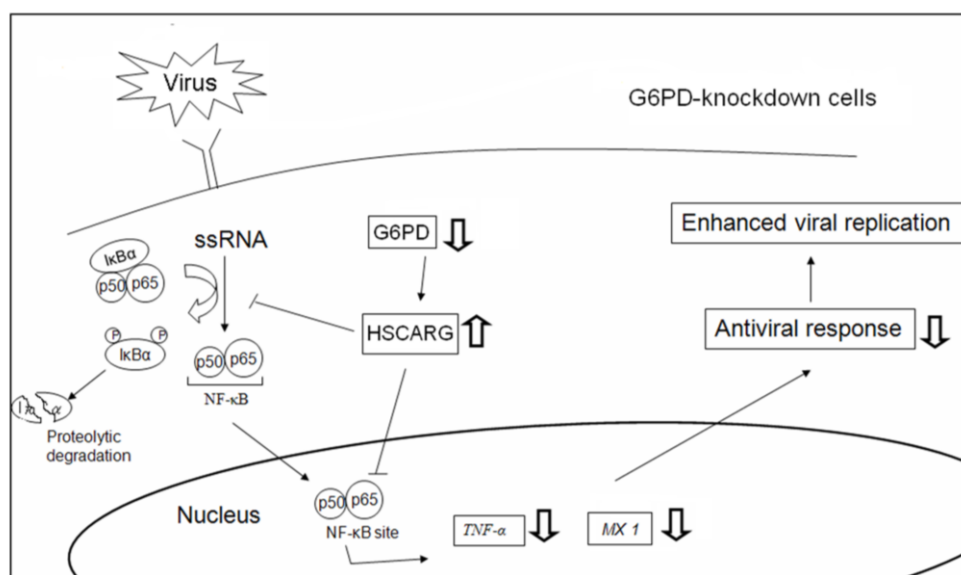


**Figure 8.** A schematic diagram shows how *G6PD* enhances antiviral response. In normal cells, viral infection induces  $I\kappa B$  degradation and  $NF-\kappa B$  translocation, which promote antiviral response and inhibit virus replication. In *G6PD*-knockdown cells, the fall in  $NADPH/NADP^+$  ratio leads to *HSCARG* upregulation, which negatively affect  $NF-\kappa B$  signaling and antiviral gene expression in response to viral infection. In this manner, viral replication is enhanced. An upward arrow indicates increase in expression or response, while a downward arrow indicates decrease in expression or response.

The transcriptional activation of  $TNF-\alpha$  and antiviral genes in virus-infected cells are mediated through a complex signaling circuitry. The  $NF-\kappa B$  signaling pathway represents an essential regulator of antiviral defense.  $NF-\kappa B$  is a key transcription factor involved in the regulation of the immune response [54–56]. It is not unprecedented that viral infection is associated with  $NF-\kappa B$  signaling, which may benefit the host or the invading microbe [57]. Infection of cells with HCoV-229E results in  $I\kappa B$  degradation and increases  $NF-\kappa B$  binding. This is accompanied by increased transcription of *TNF- $\alpha$*  and *MX1* genes, of which the promoters are endowed with  $NF-\kappa B$  binding sites. The necessity of  $NF-\kappa B$  in the activation of the antiviral response against HCoV-229E is demonstrated by the ability of BAY11-7085 to inhibit the *TNF- $\alpha$*  and *MX1* gene induction in infected cells.

$NF-\kappa B$  activation is sensitive to cellular redox changes;  $NF-\kappa B$  is normally activated under oxidative stress [58]. Paradoxically,  $NF-\kappa B$  activation is diminished in coronavirus-infected *G6PD*-deficient cells, suggesting the involvement of additional factors in the antiviral signaling pathway. *HSCARG* may act as a redox sensor, which functionally alters and undergoes differential translocation in response to different cellular  $NADPH$  levels [59]. *HSCARG* translocates from the cytoplasm to the nucleus under low  $NADPH$  conditions [38,39]. *HSCARG* has been implicated in the fine-tuning of  $NF-\kappa B$  activation. Several studies have suggested that *HSCARG* is involved in the regulation of antiviral signaling. The *HSCARG* level increases in *G6PD*-knockdown cells. Treatment with *HSCARG* siRNA increases the antiviral response and reduces the viral replication in *G6PD*-knockdown cells. It is likely that *G6PD* deficiency impairs the cellular capacity to produce

NADPH, thus enhancing HSCARG expression and its nuclear translocation. In addition, the exogenous expression of IDH1 is inhibitory to HSCARG expression. Therefore, it is conceivable that HSCARG suppresses NF- $\kappa$ B activity via modulation of I $\kappa$ B phosphorylation/degradation, leading to reduction in the expression of antiviral genes such as *TNF- $\alpha$*  and *MX1*. This reasoning may account in part for the increased susceptibility of cells to coronavirus or enterovirus. Our findings suggest that the redox status may regulate the antiviral response and viral replication via the HSCARG-NF- $\kappa$ B signaling pathway.

The clinical implications of how the G6PD status affects cellular susceptibility to viruses such as coronavirus [14], enterovirus [13], and dengue virus [15] remain to be determined. Certain clinical findings regarding individuals with G6PD-deficiency are compelling: They develop symptoms (e.g., hemolysis and pancreatitis) that are more severe after infection with the hepatitis E virus [60,61], they are more susceptible to dengue virus type 2 infection than normal subjects [15], and they develop severe pneumonia symptoms after microbial infection [62,63]. Redox imbalance may account for the impairment of antiviral immunity in patients with G6PD-deficiency. Consistent with this, interleukin-10 expression is dysregulated in monocytes from G6PD-deficient individuals [64].

The roles of G6PD in the maintenance of human health and development of disease have been extensively reviewed elsewhere [1]. Drug-induced cytotoxicity in G6PD-deficient cells is normally attributed to their reduced ability to regenerate NADPH and glutathione [4,44,65]. Deficit of NADPH can also lead to reduced NADPH oxidase activity and superoxide generation [66]. Increased superoxide generation by NADPH oxidases in diabetic mice is associated with increased G6PD activity [67]. The correlation between superoxide generation and G6PD activity has been observed in such pathophysiological situations as liver hypertrophy [68], and cardiovascular dysfunction [69]. Likewise, nitric oxide production can be affected [70]. However, the interplay between antioxidative (*i.e.*, NADPH production and maintenance of endogenous antioxidants) and pro-oxidative (*i.e.*, NADPH and superoxide production) roles of G6PD may be more complicated than previously thought. For instance, G6PD-deficient granulocytes have an impaired ability to generate superoxide, nitric oxide and hydrogen peroxide [71]. On the other hand, G6PD-deficient neutrophils show increased superoxide and hydrogen peroxide production [72]. More studies are needed to solve such a riddle.

This study demonstrates that the G6PD status modulates innate antiviral immunity via the HSCARG-NF- $\kappa$ B signaling axis. Therefore, it is likely that the G6PD status is a factor in determining the host-cell–microbe interaction.

**Supplementary Materials:** Supplementary materials can be accessed at: <http://www.mdpi.com/1999-4915/7/12/2966/s1>.

**Acknowledgments:** We are grateful to the RNAi core laboratory of Chang Gung University and National RNAi Core Facility for their technical assistance. The work was supported by grants from Chang Gung University (BMRP098, CMRPD1C0772, CMRPD1C0773, CMRPD3D0161, CMRPD3D0162, CMRPD391683, CMRPD1A0522, CMRPD1C0441, CMRPD1C0442, CMRPD1C0761, CMRPD1C0762, CMRPD190443, CMRPD1A0562, CMRPD1A0563, CMRPD1C0751, CMRPD3D0192, CMRPD1E0421, and CMRPD1C0752), the National Science Council of Taiwan (NSC101-2320-B-182-024-MY3, MOST103-2320-B-182-026-MY2, NSC99-2320-B-182-021-MY3, MOST103-2320-B-182-020, and MOST104-2320-B-182-022-MY3), the Ministry of Education of Taiwan (EMRPD1E1651, EMRPD1C0331, and EMRPD1C0281) and Chang Gung Memorial Hospital (CMRPD1B0332). The authors would like to Bill Thornton for English editing.

**Author Contributions:** Hung-Yao Ho initiated this project; Hung-Yao Ho and Daniel Tsun-Yee Chiu co-designed the initial experiments with Hung-Yao Ho specializing in viral aspect whereas Daniel Tsun-Yee Chiu specializing in G6PD and oxidative stress aspect; Yi-Hsuan Wu and Hung-Yao Ho co-designed remaining experiments; most experiments were performed by Yi-Hsuan Wu with help from Hsin-Ru Lin and Hsiang-Yu Tang; Yi-Hsuan Wu, Daniel Tsun-Yee Chiu, Mei-Ling Cheng, and Hung-Yao Ho analyzed the data; Yi-Hsuan Wu and Hung-Yao Ho wrote the first draft of the paper; Daniel Tsun-Yee Chiu, Mei-Ling Cheng, and Hung-Yao Ho gave scientific advice throughout this project and contributed significantly to manuscript revision. All authors contributed substantially to the present work, then read and approved the final manuscript.

**Conflicts of Interest:** The authors declare no conflict of interest.

## References

1. Ho, H.Y.; Cheng, M.L.; Chiu, D.T. Glucose-6-phosphate dehydrogenase—Beyond the realm of red cell biology. *Free Radic. Res.* **2014**, *48*, 1028–1048. [[CrossRef](#)] [[PubMed](#)]
2. Ho, H.Y.; Cheng, M.L.; Chiu, D.T. G6PD—An old bottle with new wine. *Chang Gung Med. J.* **2005**, *28*, 606–612. [[PubMed](#)]
3. Cheng, M.L.; Ho, H.Y.; Liang, C.M.; Chou, Y.H.; Stern, A.; Lu, F.J.; Chiu, D.T. Cellular glucose-6-phosphate dehydrogenase (G6PD) status modulates the effects of nitric oxide (NO) on human foreskin fibroblasts. *FEBS Lett.* **2000**, *475*, 257–262. [[CrossRef](#)]
4. Gao, L.P.; Cheng, M.L.; Chou, H.J.; Yang, Y.H.; Ho, H.Y.; Chiu, D.T. Ineffective GSH regeneration enhances G6PD-knockdown Hep G2 cell sensitivity to diamide-induced oxidative damage. *Free Radic. Biol. Med.* **2009**, *47*, 529–535. [[CrossRef](#)] [[PubMed](#)]
5. Ho, H.Y.; Cheng, M.L.; Lu, F.J.; Chou, Y.H.; Stern, A.; Liang, C.M.; Chiu, D.T. Enhanced oxidative stress and accelerated cellular senescence in glucose-6-phosphate dehydrogenase (G6PD)-deficient human fibroblasts. *Free Radic. Biol. Med.* **2000**, *29*, 156–169. [[CrossRef](#)]
6. Lin, C.J.; Ho, H.Y.; Cheng, M.L.; You, T.H.; Yu, J.S.; Chiu, D.T. Impaired dephosphorylation renders G6PD-knockdown HepG2 cells more susceptible to H<sub>2</sub>O<sub>2</sub>-induced apoptosis. *Free Radic. Biol. Med.* **2010**, *49*, 361–373. [[CrossRef](#)] [[PubMed](#)]
7. Arese, P.; de Flora, A. Pathophysiology of hemolysis in glucose-6-phosphate dehydrogenase deficiency. *Semin. Hematol.* **1990**, *27*, 1–40. [[PubMed](#)]
8. Sirdah, M.; Reading, N.S.; Perkins, S.L.; Shubair, M.; Aboud, L.; Prchal, J.T. Hemolysis and Mediterranean G6PD mutation (c.563 C>T) and c.1311 C>T polymorphism among Palestinians at Gaza Strip. *Blood Cells Mol. Dis.* **2012**, *48*, 203–208. [[CrossRef](#)] [[PubMed](#)]
9. Gaskin, R.S.; Estwick, D.; Peddi, R. G6PD deficiency: Its role in the high prevalence of hypertension and diabetes mellitus. *Ethn. Dis.* **2001**, *11*, 749–754. [[PubMed](#)]
10. Meloni, T.; Pacifico, A.; Forteleoni, G.; Meloni, G.F. G6PD deficiency and diabetes mellitus in northern Sardinian subjects. *Haematologica* **1992**, *77*, 94–95. [[PubMed](#)]
11. Hecker, P.A.; Leopold, J.A.; Gupte, S.A.; Recchia, F.A.; Stanley, W.C. Impact of glucose-6-phosphate dehydrogenase deficiency on the pathophysiology of cardiovascular disease. *Am. J. Physiol. Heart Circ. Physiol.* **2013**, *304*, H491–H500. [[CrossRef](#)] [[PubMed](#)]
12. Wan, G.H.; Tsai, S.C.; Chiu, D.T. Decreased blood activity of glucose-6-phosphate dehydrogenase associates with increased risk for diabetes mellitus. *Endocrine* **2002**, *19*, 191–195. [[CrossRef](#)]
13. Ho, H.Y.; Cheng, M.L.; Weng, S.F.; Chang, L.; Yeh, T.T.; Shih, S.R.; Chiu, D.T. Glucose-6-phosphate dehydrogenase deficiency enhances Enterovirus 71 infection. *J. Gen. Virol.* **2008**, *89*, 2080–2089. [[CrossRef](#)] [[PubMed](#)]
14. Wu, Y.H.; Tseng, C.P.; Cheng, M.L.; Ho, H.Y.; Shih, S.R.; Chiu, D.T. Glucose-6-phosphate dehydrogenase deficiency enhances human Coronavirus 229E infection. *J. Infect. Dis.* **2008**, *197*, 812–816. [[CrossRef](#)] [[PubMed](#)]
15. Chao, Y.C.; Huang, C.S.; Lee, C.N.; Chang, S.Y.; King, C.C.; Kao, C.L. Higher infection of Dengue virus serotype 2 in human monocytes of patients with G6PD deficiency. *PLoS ONE* **2008**, *3*, e1557. [[CrossRef](#)] [[PubMed](#)]
16. Goodbourn, S.; Didcock, L.; Randall, R.E. Interferons: Cell signalling, immune modulation, antiviral response and virus countermeasures. *J. Gen. Virol.* **2000**, *81*, 2341–2364. [[CrossRef](#)] [[PubMed](#)]
17. McFadden, G.; Mohamed, M.R.; Rahman, M.M.; Barte, E. Cytokine determinants of viral tropism. *Nat. Rev. Immunol.* **2009**, *9*, 645–655. [[CrossRef](#)] [[PubMed](#)]
18. Matikainen, S.; Siren, J.; Tissari, J.; Veckman, V.; Pirhonen, J.; Severa, M.; Sun, Q.; Lin, R.; Meri, S.; Uze, G.; *et al.* Tumor necrosis factor  $\alpha$  enhances influenza A virus-induced expression of antiviral cytokines by activating RIG-I gene expression. *J. Virol.* **2006**, *80*, 3515–3522. [[CrossRef](#)] [[PubMed](#)]
19. Barte, E.; Mohamed, M.R.; McFadden, G. Tumor necrosis factor and interferon: Cytokines in harmony. *Curr. Opin. Microbiol.* **2008**, *11*, 378–383. [[CrossRef](#)] [[PubMed](#)]
20. Sadler, A.J.; Williams, B.R. Interferon-inducible antiviral effectors. *Nat. Rev. Immunol.* **2008**, *8*, 559–568. [[CrossRef](#)] [[PubMed](#)]

21. Justesen, J.; Hartmann, R.; Kjeldgaard, N.O. Gene structure and function of the 2'-5'-oligoadenylate synthetase family. *Cell Mol. Life Sci.* **2000**, *57*, 1593–1612. [[CrossRef](#)] [[PubMed](#)]
22. Malathi, K.; Paranjape, J.M.; Bulanova, E.; Shim, M.; Guenther-Johnson, J.M.; Faber, P.W.; Eling, T.E.; Williams, B.R.; Silverman, R.H. A transcriptional signaling pathway in the IFN system mediated by 2'-5'-oligoadenylate activation of RNase L. *Proc. Natl. Acad. Sci. USA* **2005**, *102*, 14533–14538. [[CrossRef](#)] [[PubMed](#)]
23. Verhelst, J.; Parthoens, E.; Schepens, B.; Fiers, W.; Saelens, X. Interferon-inducible protein Mx1 inhibits influenza virus by interfering with functional viral ribonucleoprotein complex assembly. *J. Virol.* **2012**, *86*, 13445–13455. [[CrossRef](#)] [[PubMed](#)]
24. Elde, N.C.; Child, S.J.; Eickbush, M.T.; Kitzman, J.O.; Rogers, K.S.; Shendure, J.; Geballe, A.P.; Malik, H.S. Poxviruses deploy genomic accordions to adapt rapidly against host antiviral defenses. *Cell* **2012**, *150*, 831–841. [[CrossRef](#)] [[PubMed](#)]
25. Zhao, L.; Birdwell, L.D.; Wu, A.; Elliott, R.; Rose, K.M.; Phillips, J.M.; Li, Y.; Grinspan, J.; Silverman, R.H.; Weiss, S.R. Cell-type-specific activation of the oligoadenylate synthetase-RNase L pathway by a murine coronavirus. *J. Virol.* **2013**, *87*, 8408–8418. [[CrossRef](#)] [[PubMed](#)]
26. Zorzitto, J.; Galligan, C.L.; Ueng, J.J.; Fish, E.N. Characterization of the antiviral effects of interferon- $\alpha$  against a SARS-like coronavirus infection *in vitro*. *Cell Res.* **2006**, *16*, 220–229. [[CrossRef](#)] [[PubMed](#)]
27. Leong, W.F.; Tan, H.C.; Ooi, E.E.; Koh, D.R.; Chow, V.T. Microarray and real-time RT-PCR analyses of differential human gene expression patterns induced by severe acute respiratory syndrome (SARS) coronavirus infection of Vero cells. *Microbes Infect.* **2005**, *7*, 248–259. [[CrossRef](#)] [[PubMed](#)]
28. Ida-Hosonuma, M.; Iwasaki, T.; Yoshikawa, T.; Nagata, N.; Sato, Y.; Sata, T.; Yoneyama, M.; Fujita, T.; Taya, C.; Yonekawa, H.; *et al.* The  $\alpha/\beta$  interferon response controls tissue tropism and pathogenicity of poliovirus. *J. Virol.* **2005**, *79*, 4460–4469. [[CrossRef](#)] [[PubMed](#)]
29. Kim, S.Y.; Solomon, D.H. Tumor necrosis factor blockade and the risk of viral infection. *Nat. Rev. Rheumatol.* **2010**, *6*, 165–174. [[CrossRef](#)] [[PubMed](#)]
30. Alfadda, A.A.; Sallam, R.M. Reactive oxygen species in health and disease. *J. Biomed. Biotechnol.* **2012**, *2012*, 936486. [[CrossRef](#)] [[PubMed](#)]
31. Groeger, G.; Quiney, C.; Cotter, T.G. Hydrogen peroxide as a cell-survival signaling molecule. *Antioxid. Redox Signal.* **2009**, *11*, 2655–2671. [[CrossRef](#)] [[PubMed](#)]
32. Bedard, K.; Krause, K.H. The NOX family of ROS-generating NADPH oxidases: Physiology and pathophysiology. *Physiol. Rev.* **2007**, *87*, 245–313. [[CrossRef](#)] [[PubMed](#)]
33. Rada, B.; Leto, T.L. Oxidative innate immune defenses by Nox/Duox family NADPH oxidases. *Contrib. Microbiol.* **2008**, *15*, 164–187. [[PubMed](#)]
34. Grandvaux, N.; Soucy-Faulkner, A.; Fink, K. Innate host defense: Nox and Duox on phox's tail. *Biochimie* **2007**, *89*, 1113–1122. [[CrossRef](#)] [[PubMed](#)]
35. Dolowschiak, T.; Chassin, C.; Ben Mkaddem, S.; Fuchs, T.M.; Weiss, S.; Vandewalle, A.; Hornef, M.W. Potentiation of epithelial innate host responses by intercellular communication. *PLoS Pathog.* **2010**, *6*, e1001194. [[CrossRef](#)] [[PubMed](#)]
36. Soucy-Faulkner, A.; Mukawera, E.; Fink, K.; Martel, A.; Jouan, L.; Nzengue, Y.; Lamarre, D.; Vande Velde, C.; Grandvaux, N. Requirement of NOX2 and reactive oxygen species for efficient RIG-I-mediated antiviral response through regulation of MAVS expression. *PLoS Pathog.* **2010**, *6*, e1000930. [[CrossRef](#)] [[PubMed](#)]
37. Dai, X.; Li, Y.; Meng, G.; Yao, S.; Zhao, Y.; Yu, Q.; Zhang, J.; Luo, M.; Zheng, X. NADPH is an allosteric regulator of HSCARG. *J. Mol. Biol.* **2009**, *387*, 1277–1285. [[CrossRef](#)] [[PubMed](#)]
38. Zheng, X.; Dai, X.; Zhao, Y.; Chen, Q.; Lu, F.; Yao, D.; Yu, Q.; Liu, X.; Zhang, C.; Gu, X.; *et al.* Restructuring of the dinucleotide-binding fold in an NADP(H) sensor protein. *Proc Natl Acad Sci USA* **2007**, *104*, 8809–8814. [[CrossRef](#)] [[PubMed](#)]
39. Lian, M.; Zheng, X. HSCARG regulates NF- $\kappa$ B activation by promoting the ubiquitination of RelA or COMMD1. *J. Biol. Chem.* **2009**, *284*, 17998–18006. [[CrossRef](#)] [[PubMed](#)]
40. Gan, Q.; Li, T.; Hu, B.; Lian, M.; Zheng, X. HSCARG inhibits activation of NF- $\kappa$ B by interacting with I $\kappa$ B kinase- $\beta$ . *J. Cell Sci.* **2009**, *122 Pt 22*, 4081–4088. [[CrossRef](#)] [[PubMed](#)]
41. Zhang, M.; Hu, B.; Li, T.; Peng, Y.; Guan, J.; Lai, S.; Zheng, X. A CRM1-dependent nuclear export signal controls nucleocytoplasmic translocation of HSCARG, which regulates NF- $\kappa$ B activity. *Traffic* **2012**, *13*, 790–799. [[CrossRef](#)] [[PubMed](#)]



42. Peng, Y.; Xu, R.; Zheng, X. HSCARG negatively regulates the cellular antiviral RIG-I like receptor signaling pathway by inhibiting TRAF3 ubiquitination via recruiting OTUB1. *PLoS Pathog.* **2014**, *10*, e1004041. [[CrossRef](#)] [[PubMed](#)]
43. Lin, H.R.; Wu, C.C.; Wu, Y.H.; Hsu, C.W.; Cheng, M.L.; Chiu, D.T. Proteome-wide dysregulation by glucose-6-phosphate dehydrogenase (G6PD) reveals a novel protective role for G6PD in aflatoxin B(1)-mediated cytotoxicity. *J. Proteome Res.* **2013**, *12*, 3434–3448. [[CrossRef](#)] [[PubMed](#)]
44. Ho, H.Y.; Cheng, M.L.; Shiao, M.S.; Chiu, D.T. Characterization of global metabolic responses of glucose-6-phosphate dehydrogenase-deficient hepatoma cells to diamide-induced oxidative stress. *Free Radic. Biol. Med.* **2013**, *54*, 71–84. [[CrossRef](#)] [[PubMed](#)]
45. Cho, M.K.; Jang, Y.P.; Kim, Y.C.; Kim, S.G. Arctigenin, a phenylpropanoid dibenzylbutyrolactone lignan, inhibits MAP kinases and AP-1 activation via potent MKK inhibition: The role in TNF- $\alpha$  inhibition. *Int. Immunopharmacol.* **2004**, *4*, 1419–1429. [[CrossRef](#)] [[PubMed](#)]
46. Holzinger, D.; Jorns, C.; Stertz, S.; Boisson-Dupuis, S.; Thimme, R.; Weidmann, M.; Casanova, J.L.; Haller, O.; Kochs, G. Induction of MxA gene expression by influenza A virus requires type I or type III interferon signaling. *J. Virol.* **2007**, *81*, 7776–7785. [[CrossRef](#)] [[PubMed](#)]
47. Ho, H.Y.; Cheng, M.L.; Chiu, D.T. Glucose-6-phosphate dehydrogenase—From oxidative stress to cellular functions and degenerative diseases. *Redox Rep.* **2007**, *12*, 109–118. [[CrossRef](#)] [[PubMed](#)]
48. Tisoncik, J.R.; Billharz, R.; Burmakina, S.; Belisle, S.E.; Proll, S.C.; Korth, M.J.; Garcia-Sastre, A.; Katze, M.G. The NS1 protein of influenza A virus suppresses interferon-regulated activation of antigen-presentation and immune-proteasome pathways. *J. Gen. Virol.* **2011**, *92*, 2466. [[CrossRef](#)]
49. Sharma, K.; Tripathi, S.; Ranjan, P.; Kumar, P.; Garten, R.; Deyde, V.; Katz, J.M.; Cox, N.J.; Lal, R.B.; Sambhara, S.; *et al.* Influenza A virus nucleoprotein exploits Hsp40 to inhibit PKR activation. *PLoS ONE* **2011**, *6*, e20215. [[CrossRef](#)] [[PubMed](#)]
50. Wang, G.; Chen, G.; Zheng, D.; Cheng, G.; Tang, H. PLP2 of mouse hepatitis virus A59 (MHV-A59) targets TBK1 to negatively regulate cellular type I interferon signaling pathway. *PLoS ONE* **2011**, *6*, e17192. [[CrossRef](#)] [[PubMed](#)]
51. Lu, X.; Pan, J.; Tao, J.; Guo, D. SARS-CoV nucleocapsid protein antagonizes IFN- $\beta$  response by targeting initial step of IFN- $\beta$  induction pathway, and its C-terminal region is critical for the antagonism. *Virus Genes* **2011**, *42*, 37–45. [[CrossRef](#)] [[PubMed](#)]
52. Antoniak, S.; Owens, A.P., 3rd; Baunacke, M.; Williams, J.C.; Lee, R.D.; Weithauser, A.; Sheridan, P.A.; Malz, R.; Luyendyk, J.P.; Esserman, D.A.; *et al.* PAR-1 contributes to the innate immune response during viral infection. *J. Clin. Investig.* **2013**, *123*, 1310–1322. [[CrossRef](#)] [[PubMed](#)]
53. Bendelja, K.; Vojvoda, V.; Aberle, N.; Cepin-Bogovic, J.; Gagro, A.; Mlinaric-Galinovic, G.; Rabatic, S. Decreased Toll-like receptor 8 expression and lower TNF- $\alpha$  synthesis in infants with acute RSV infection. *Respir. Res.* **2010**, *11*, 143. [[CrossRef](#)] [[PubMed](#)]
54. Hiscott, J.; Grandvaux, N.; Sharma, S.; Tenoever, B.R.; Servant, M.J.; Lin, R. Convergence of the NF- $\kappa$ B and interferon signaling pathways in the regulation of antiviral defense and apoptosis. *Ann. N. Y. Acad. Sci.* **2003**, *1010*, 237–248. [[CrossRef](#)] [[PubMed](#)]
55. Hiscott, J. Convergence of the NF- $\kappa$ B and IRF pathways in the regulation of the innate antiviral response. *Cytokine Growth Factor Rev.* **2007**, *18*, 483–490. [[CrossRef](#)] [[PubMed](#)]
56. Akira, S. TLR signaling. *Curr. Top. Microbiol. Immunol.* **2006**, *311*, 1–16. [[PubMed](#)]
57. Santoro, M.G.; Rossi, A.; Amici, C. NF- $\kappa$ B and virus infection: Who controls whom. *EMBO J.* **2003**, *22*, 2552–2560. [[CrossRef](#)] [[PubMed](#)]
58. Siomek, A. NF- $\kappa$ B signaling pathway and free radical impact. *Acta Biochim. Pol.* **2012**, *59*, 323–331. [[PubMed](#)]
59. Lamb, H.K.; Stammers, D.K.; Hawkins, A.R. Dinucleotide-sensing proteins: Linking signaling networks and regulating transcription. *Sci. Signal.* **2008**, *1*, pe38. [[CrossRef](#)] [[PubMed](#)]
60. Thapa, R.; Biswas, B.; Mallick, D.; Ghosh, A. Acute pancreatitis—Complicating hepatitis E virus infection in a 7-year-old boy with glucose 6 phosphate dehydrogenase deficiency. *Clin. Pediatr.* **2009**, *48*, 199–201. [[CrossRef](#)] [[PubMed](#)]
61. Au, W.Y.; Ngai, C.W.; Chan, W.M.; Leung, R.Y.; Chan, S.C. Hemolysis and methemoglobinemia due to hepatitis E virus infection in patient with G6PD deficiency. *Ann. Hematol.* **2011**, *90*, 1237–1238. [[CrossRef](#)] [[PubMed](#)]

62. Nowinski, A.; Jablonska-Skwiecinska, E.; Wojda, E.; Bielen, P.; Ptak, J.; Sliwinski, P.; Gorecka, D. Community-acquired pneumonia complications in a patient with hereditary glucose-6-phosphate dehydrogenase deficiency. *Pneumonol. Alergol. Pol.* **2007**, *75*, 283–288. [[PubMed](#)]
63. Douzinas, E.E.; Flevari, K.; Andrianakis, I.; Betrosian, A.P. Oral atovaquone for the treatment of severe *Pneumocystis jirovecii* pneumonia in a patient with glucose-6-phosphate dehydrogenase deficiency. *Scand. J. Infect. Dis.* **2010**, *42*, 76–78. [[CrossRef](#)] [[PubMed](#)]
64. Santos, S.S.; Brunialti, M.K.; Rigato, O.; Machado, F.R.; Silva, E.; Salomao, R. Generation of nitric oxide and reactive oxygen species by neutrophils and monocytes from septic patients and association with outcomes. *Shock* **2012**, *38*, 18–23. [[CrossRef](#)] [[PubMed](#)]
65. Tang, H.Y.; Ho, H.Y.; Wu, P.R.; Chen, S.H.; Kuypers, F.A.; Cheng, M.L.; Chiu, D.T. Inability to maintain GSH pool in G6PD-deficient red cells causes futile AMPK activation and irreversible metabolic disturbance. *Antioxid. Redox Signal.* **2015**, *22*, 744–759. [[CrossRef](#)] [[PubMed](#)]
66. Yang, H.C.; Cheng, M.L.; Ho, H.Y.; Chiu, D.T. The microbicidal and cyto regulatory roles of NADPH oxidases. *Microbes Infect. Inst. Pasteur* **2011**, *13*, 109–120. [[CrossRef](#)] [[PubMed](#)]
67. Serpillon, S.; Floyd, B.C.; Gupte, R.S.; George, S.; Kozicky, M.; Neito, V.; Recchia, F.; Stanley, W.; Wolin, M.S.; Gupte, S.A. Superoxide production by NAD(P)H oxidase and mitochondria is increased in genetically obese and hyperglycemic rat heart and aorta before the development of cardiac dysfunction. The role of glucose-6-phosphate dehydrogenase-derived NADPH. *Am. J. Physiol. Heart Circ. Physiol.* **2009**, *297*, H153–H162. [[CrossRef](#)] [[PubMed](#)]
68. Gupte, R.S.; Floyd, B.C.; Kozicky, M.; George, S.; Ungvari, Z.I.; Neito, V.; Wolin, M.S.; Gupte, S.A. Synergistic activation of glucose-6-phosphate dehydrogenase and NAD(P)H oxidase by Src kinase elevates superoxide in type 2 diabetic, Zucker *fa/fa*, rat liver. *Free Radic. Biol. Med.* **2009**, *47*, 219–228. [[CrossRef](#)] [[PubMed](#)]
69. Gupte, S.A. Glucose-6-phosphate dehydrogenase: A novel therapeutic target in cardiovascular diseases. *Curr. Opin. Investig. Drugs* **2008**, *9*, 993–1000. [[PubMed](#)]
70. Stanton, R.C. Glucose-6-phosphate dehydrogenase, NADPH, and cell survival. *IUBMB Life* **2012**, *64*, 362–369. [[CrossRef](#)] [[PubMed](#)]
71. Tsai, K.J.; Hung, I.J.; Chow, C.K.; Stern, A.; Chao, S.S.; Chiu, D.T. Impaired production of nitric oxide, superoxide, and hydrogen peroxide in glucose 6-phosphate-dehydrogenase-deficient granulocytes. *FEBS Lett.* **1998**, *436*, 411–414. [[CrossRef](#)]
72. Cheng, M.L.; Ho, H.Y.; Lin, H.Y.; Lai, Y.C.; Chiu, D.T. Effective NET formation in neutrophils from individuals with G6PD Taiwan-Hakka is associated with enhanced NADP<sup>+</sup> biosynthesis. *Free Radic. Res.* **2013**, *47*, 699–709. [[CrossRef](#)] [[PubMed](#)]



© 2015 by the authors; licensee MDPI, Basel, Switzerland. This article is an open access article distributed under the terms and conditions of the Creative Commons by Attribution (CC-BY) license (<http://creativecommons.org/licenses/by/4.0/>).